Review

A Critical Review of Recent Inorganic Redox Flow Batteries Development from Laboratories to Industrial Applications

Chivukula Kalyan Sundar Krishna [ID] and Yansong Zhao *[ID]

Department of Safety, Chemistry and Biomedical Laboratory Sciences, Western Norway University of Applied Sciences (HVL), 5063 Bergen, Norway; ckri@hvl.no
* Correspondence: yansong.zhao@hvl.no

Abstract

Redox flow batteries (RFBs) are an emerging class of large-scale energy storage devices, yet the commercial benchmark—vanadium redox flow batteries (VRFBs)—is highly constrained by a modest open-circuit potential (1.26 V) while posing an expensive and volatile material procurement costs. This review focuses on recent progress in diversifying redox-active species to overcome these limits, highlighting chemistries that increase overall cell voltage, energy density, and efficiency while maintaining long cycle life and safety. The study dwells deeper into manganese-based systems (e.g., Mn/Ti, Mn/V, Mn/S, M/Zn) that leverage Mn's high positive potential while addressing Mn(III) disproportionation reactions; iron-based hybrids (Fe/Cr, Fe/Zn, Fe/Pb, Fe/V, Fe/S, Fe/Cd) that exploit the low cost, and its abundance, along with membrane and electrolyte strategies to prevent the potential issue involving crossover; cerium-anchored catholytes (Ce/Pb, V/Ce, Eu/Ce, Ce/S, Ce/Zn) that deliver high operational voltage by implementing an acid-base media, along with selective zeolite membranes; and halide systems (Zn–I, Zn–Br, Sn–Br, polysulfide–bromine/iodide) that combine fast redox kinetics and high solubility with advances such as carbon-coated membranes, bromine complexation, and ambipolar electrolytes. Across these various families of RFBs, the review highlights the modifications made to the flow-fields, membranes, and electrodes by utilizing a zero-gap serpentine flow field, sulfonated poly(ether ether ketone) (SPEEK) membranes, carbon-modified and zeolite separators, electrolyte additives to enhance the voltage (VE%), and thereby energy (EE%) efficiency, while reducing the overall system cost. These modifications to the existing RFB technology offer a promising alternative to traditional approaches, paving the way for improved performance and widespread adoption of RFB technology in large-scale grid-based energy storage solutions.

Keywords: redox flow battery; inorganic; energy density; inexpensive; high voltage

1. Introduction

The urgent need for a high-energy-density electrochemical storage device has been a major focus in recent years, driven by the growth of renewable energy storage. Due to the passage of the peak oil point, the production and utilization of natural gas are rather unprofitable and pose an imminent threat to the environment. In this regard, the utilization of renewable energy has been put forth due to its ever-lasting energy production and environmentally friendly nature.

However, renewable energy is rather sporadic in nature and not reliable for continuous energy storage. To tackle this, a variety of energy storage devices have been developed,

including but not limited to supercapacitors, batteries, and fuel cells. [1–11]. Of these, batteries exhibit optimal energy and power densities, making them a promising candidate for use in grid-scale energy storage solutions. Of the various types of batteries currently commercialized in the marketplace, lithium-ion batteries [4,5,7] occupy the majority of the market share due to their excellent working potentials, energy, and power densities without compromising on the efficiencies. However, on a larger scale, the deployment of Li-ion batteries is rather non-profitable and poses several challenges to the environment, post-utilization of the battery. To tackle these issues and to effectively utilize the grid-scale harnessed energy, redox flow batteries (RFBs) have been introduced to the marketplace, with vanadium redox flow batteries (VRFBs) leading the way. A typical VRFB lasts for more than 30,000 charge-discharge cycles, compared to a Li-ion battery, which runs for only 500–1000 cycles. Moreover, post-utilization of the RFB, the electrolytes can be regenerated and re-utilized, eliminating the risks of potential waste discharge to the environment. However, the currently commercialized VRFBs possess a lower working potential of 1.26 V as compared to the 3.4 V Li-ion battery, limiting their overall energy density.

A RFB primarily consists of two external chambers filled with liquid electrolyte which continuously flows into a cell commonly consisting of a porous carbon felt, and graphite plates, for the liquid electrolyte to soak, and to aid in the electron transfer through the external circuit with the help of graphite plates, and an ion-exchange membrane to facilitate the transfer of protons across the two chambers of the cell. The positive and negative electrolyte regions are termed catholyte and anolyte, respectively, and are prevented from cross-mixing by the ion-exchange membrane, rather than a separator as seen in a Li-ion battery. The schematic of a simplified redox flow battery is illustrated in Figure 1.
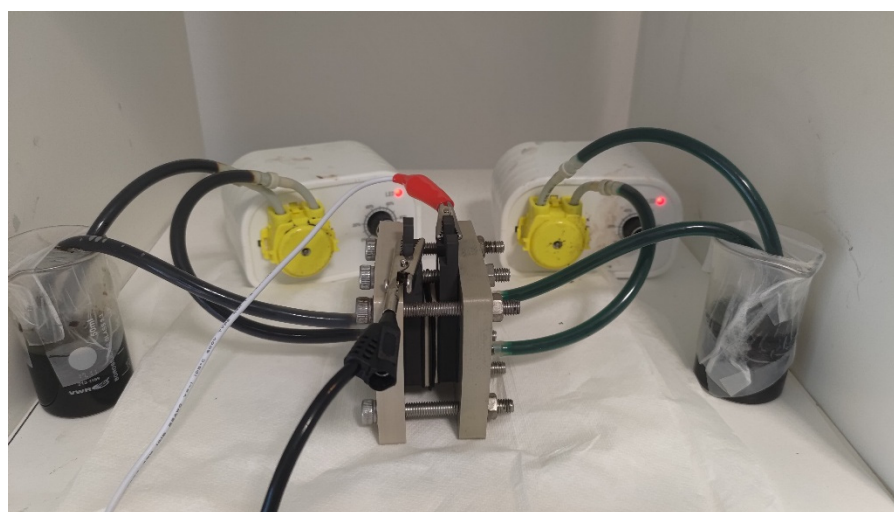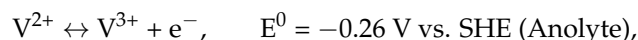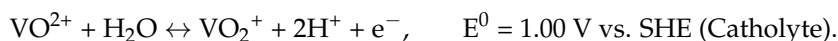

Figure 1. A schematic of a lab-scale vanadium redox flow battery [12].

In commercialized VRFBs, catholyte consists of vanadium in +4 (discharged) and +5 (charged) oxidation states, while the anolyte comprises +2 (charged) and +3 (discharged) oxidation states. Moreover, since it is an all-vanadium RFB, the scope for cross-contamination is rather negligible, unlike the previously developed RFBs utilizing the couples Fe-Cr and Br-polysulphide, etc. [13,14]. In a typical VRFB, vanadyl sulphate ($VOSO_4$) is dissolved in 3 M H_2SO_4 solution, and the same solution is utilized as catholyte and anolyte in the RFB. Due to the presence of a +4 oxidation state in both electrolytes, there is no driving force for the electron transfer. So, during the first cycle, the electrolytes are typically charged at 1.5 V to reach their respective oxidation states, i.e., +5 in the catholyte and +2 in the anolyte, to provide the driving force for electron transfer during discharge. During the charging process, V^{4+} gets soaked on the carbon felt, and upon interacting with the graphite

plates, to which the external cables are connected as shown in Figure 1, it releases electrons through the outer circuit. Furthermore, to maintain the charge balance, the positively charged protons (H^+) exchange through the proton exchange membrane inside the cell. The reactions occurring at the graphite plates, along with their standard potentials, are as follows:

$$V^{2+} \leftrightarrow V^{3+} + e^-, \qquad E^0 = -0.26 \text{ V vs. SHE (Anolyte)},$$

and

$$VO^{2+} + H_2O \leftrightarrow VO_2{}^+ + 2H^+ + e^-, \qquad E^0 = 1.00 \text{ V vs. SHE (Catholyte)}.$$

The open circuit potential (OCP) of the vanadium redox flow batteries results in $1 - (-0.25) = 1.25$ V, and the overall reaction is as follows,

$$VO^{2+} + H_2O + V^{3+} \leftrightarrow VO_2{}^+ + V^{2+} + 2H^+, \qquad E^{OCP} = 1.25 \text{ V (theoretical)}$$
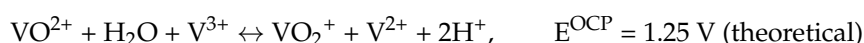
Moreover, in addition to these primary reactions, side reactions include the generation of hydrogen and oxygen gases, which can negatively impact the performance of the battery. The hydrogen evolution reaction (HER) and oxygen evolution reactions (OER) by electrolyzing the solvent, viz. DI-water, as follows:

$$2H^+ + 2e^- \leftrightarrow H_2$$

and

$$2H_2O \leftrightarrow O_2 + 4H^+ + 4e^-$$
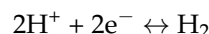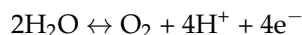
On assuming there are no side reactions, the Nernst equation can be utilized to calculate the voltage of the cell as $E = E^* + \frac{RT}{F}\ln\left[\frac{\alpha_{pr}}{\alpha_{re}}\right]$. Here, α_{pr} and α_{re} represent the activity of products and reactants, respectively. However, despite their numerous advantages, the widespread adoption of VRFBs at grid scale remains limited due to their relatively low OCP, solubility of their salts in the aqueous solutions, and the price volatility of vanadium resources. Since the energy stored in an RFB is inherently tied to the working potential between the redox couples and their reversible redox kinetics, there is a pressing need to explore alternative chemistries that can deliver higher voltages and improved electrochemical performances.

In recent years, significant research efforts have been directed toward modifying the electrolytes and thereby expanding the redox landscape of the flow battery technology by introducing a wide range of non-vanadium redox-active species, including organic, inorganic, semi-solid, and nonaqueous redox couples [15–25]. These innovations aim to broaden the electrochemical stability window, thereby enhancing the overall OCP and energy efficiency of RFBs. Such diversification not only improves energy density but also offers opportunities to reduce system costs by lowering the inherent material procurement expenses. However, one of the major challenges facing non-aqueous RFBs lies in the development of a suitable ion-transport membrane. Traditional ion-exchange membranes such as Nafion or SPEEK, which effectively conduct H^+ ions in aqueous systems, are not compatible with non-aqueous electrolytes, due to the lack of freely available protons and the reduced ionic conductivity of most organic solvents. To address this limitation, various studies have explored the replacement of proton exchange mechanisms with a specific cation-selective membrane designed for alternative charge carriers such as Li^+, Na^+, or K^+ ions, in conjunction with suitable supporting salts such as KCl, NaCl, $LiClO_4$, in the electrolyte medium, to maintain the charge balance. Despite encouraging progress, membrane optimization for non-aqueous systems remains a key bottleneck toward their practical deployment in the grid-scale energy storage solutions.

In this context, the present review article focuses specifically on inorganic aqueous RFB chemistries, where the interplay between redox-active materials and the membrane-mediated ion transport is well established. The review emphasizes how strategic selection and pairing of redox couples can maximize the operational voltage window and thereby enhance the energy density and long-term performance of aqueous RFB systems. While numerous studies [24,26,27] have explored individual chemistries utilizing organic/inorganic redox active materials, beyond the traditional vanadium-based systems, a unified representation on how these redox couples relate in enhancing the OCP, energy density, and pairing strategy remains rather limited, all while incorporating non-toxic and inexpensive materials. This review addresses the gap by systematically examining the evolution of a particular class of flow battery technology with a significant potential to replace the VRFBs on a grid-scale basis—inorganic aqueous RFBs. Identifying which redox couples exhibit the highest standard reduction potentials and outlining the principles for pairing catholyte and anolyte species to maximize OCP without compromising stability, reversibility, or cost, aids in advancing the research of inorganic aqueous RFBs—beyond vanadium—towards commercialization. Among the various emerging systems, cerium, iron, manganese, titanium, and halide or polysulfide-based chemistries stand out for their favourable redox properties and material abundance. The following sections of the manuscript delve deeper into the development of various types of redox flow batteries, exploring their fundamental mechanisms, performance characteristics, and recent innovations.

2. Manganese-Based RFBs

Manganese (Mn), being the 12th most abundant mineral in the Earth's crust, along with its ability to showcase a broad range of oxidation states with significantly higher potential as compared to vanadium, numerous studies focused primarily on utilizing 'Mn' as the catholyte [28–42]. However, the rapid growth of Mn-based RFBs has been restricted due to the precipitation of MnO_2, which in turn acts as a blockage leading to the pressure buildup, and eventually breakage of the RFB. To overcome this issue and to extract the high redox potential of Mn, numerous studies have been performed. While the standard reduction potential (SHE) of Mn^{3+}/Mn^{2+} is 1.5 V (greater than 1 V vs. SHE when compared to vanadium), coupling the catholyte consisting of Mn with an anolyte exhibiting the potentials in a similar range would significantly aid in enhancing the overall energy density of the RFB. In this regard, Liu et al., [33] utilized $ZnCl_2$ as the catholyte and $MnCl_2$ as the catholyte solution in the presence of a series of environmentally friendly amino acid derivatives, namely, L-Amine, L-Valine, and Glycine, which aid in the suppression of Cl_2 evolution due to the formation of hydron bonding. Amongst the various amino acid derivatives, glycine showcased a stable charge-discharge performance, along with the suppression of chlorine gas, which was later incorporated into the hybrid Zn-Mn RFB ($Gly:MnCl_2 = 1:1$) to evaluate its overall electrochemical performance. As opposed to a conventional RFB, wherein both half-cell reactions involve soluble redox-active species that remain dissolved throughout charge and discharge processes, hybrid flow batteries (HFBs) combine one soluble redox couple with a solid-phase redox process. These flow batteries typically involve electrodeposition and stripping of a metal at one electrode (e.g., Zn, Pb, Cd, or Cu). The hybrid RFBs share a similar flow-based electrolyte design; however, they differ in the energy storage mechanism, viz., energy is stored in the solid electrode phase in one half-cell.

The presence of glycine in the hybrid zinc manganese RFB aided in improving the binding energy of gly-Mn^{2+} as compared to Mn^{2+}-H_2O, resulting in the inhibition of precipitate formation and enhancing the overall life cycle and efficiency of the hybrid ZMRFB [33].

The overall OCP of the hybrid ZMRFB showcased a value of approximately 2.0 V, with a discharge plateau around 1.6 V. However, as stated by numerous studies, the primary issue of concern in relation to the Mn-based flow batteries is the dissociation of Mn^{3+} into Mn^{2+} and MnO_2 (precipitates), causing a severe problem of capacity fading. This has been documented to be subsided by the presence of TiO^{2+} or V^{5+} ions in the electrolyte region by Reynard et al. [35]. The presence of these ions aids in shifting the reaction equilibrium away from the production of MnO_2 by the formation of complexes with Mn, thus inhibiting the undesired step, viz. Mn^{3+} disproportion into Mn^{2+} and MnO_2. Following this, in the spirit of incorporating a different anolyte to achieve higher energy densities, while retaining Mn-based catholyte due to its high redox potential (1.5 V vs. SHE), vanadium-based anolyte has been utilized to assess its influence, and thereby the overall electrochemical performance of the VMRFB. The study performed by Chakrabarti et al., [29] utilized Ti^{4+} as a complexing agent to inhibit the disproportion reaction, thereby enhancing the overall energy storage capacity of the VMRFB, along with electrospun carbon metal fabrics (CMFs) in combination with thermally activated graphite felt control rods as the electrode. The obtained results have been compared with the commercialized VRFB setup to evaluate the potential of utilizing VMRFB in large-scale energy storage devices.

Along similar lines of utilizing Mn's high redox potential of 1.5 V vs. SHE and a cheaper alternative as compared to vanadium, Dong et al., [40] introduced the concept of utilizing titanium as an anolyte, resulting in a novel manganese—titanium RFB (MTRFB). Furthermore, the RFB employed a mixed electrolyte alternative to eliminate the potential threat of electrolyte crossover and contamination. The developed MTRFB showcased an OCP of 1.55 V and an energy density of 23.5 Wh L^{-1}. Furthermore, the RFB displayed a coulombic (CE%), voltage (VE%), and energy efficiencies (EE%) of 99.8%, 86.9%, and 86.7%, respectively, for more than 40 cycles of operation, indicating the stability of titanium and its potential application in RFB technology. Along similar lines of utilizing titanium as an anolyte, and to reduce the formation of MnO_2 during the discharge regime of manganese-based RFBs, M. Nan et al., [34] incorporated a charge-induced slurry (CMRFB). This demonstrated the utilization of MnO_2 nanoparticles as the redox active materials, and thereby subsiding the disproportionation reaction, leading to the formation of precipitation. The resulting flow battery exhibited a CE%, VE%, and EE% of 99%, 86%, and 85% at a discharge current of 40 mA cm^{-2} for greater than 1000 cycles of operation, indicating the stability. The incorporation of the charge-induced slurry mechanism showcased an effective minimization of the imminent and persistent problem in manganese-based flow batteries.

In order to further reduce the cost of active materials, and to enhance the overall OCP of the Mn-based RFBs, a few studies have focused on utilizing polysulphides [30,32] as the anolyte solution due to their high redox potential, viz. 0.51 V vs. SHE. However, the chemistry governing the utilization of polysulfides in aqueous RFBs is inherently complex, primarily due to the dynamic equilibrium between long-chained (S_n^{2-}, n > 4) and short-chained (S_n^{2-}, n < 4) species that form during the charge-discharge of the battery. The distribution of these species depends strongly on several factors, including the composition of the anolyte solution, the alkalinity of the electrolyte, and the stoichiometry of elemental sulphur to sulphide salts (e.g., Na_2S or K_2S). The addition of a suitable base, such as KOH or NaOH, is quite essential to suppress the evolution of toxic H_2S gas and to stabilize the dissolved polysulfide species. Increasing the proportion of elemental sulphur in the anolyte promotes the formation of longer-chain polysulfides (S_6^{2-}–S_8^{2-}), which can initially enhance sulphur utilization but also increase the disproportionation reactions that yield shorter species (S_2^{2-}, S_3^{2-}). This phenomenon of interconversion between the long and short-chain polysulphides leads to self-discharge and capacity fading, lowering the CE%. The process of oxidation and reduction of polysulphides

has been well-documented by utilizing an operando UV-VIS spectroscopy technique, to determine the presence of long and short-chained polysulphides at various potentials in a polysulphide–iodide–based RFB setup by Li et al. [43].

In the study performed on Mn-S RFB [32], the Mn-based electrolyte is utilized as a catholyte solution, and the alkaline solution of polysulphides is used as the anolyte solution, with a charged reinforced K^+ ion type modified Nafion membrane has been incorporated into the RFB to maintain the charge balance. Furthermore, Ni-foil has been utilized rather than carbon felt on the anolyte side of the MSRFB, whereas pretreated carbon felt was used for the catholyte section. Thus prepared RFB was studied under various current densities ranging from 5 to 40 mA cm^{-2}, and the MSRFB showcased a CE% of greater than 95% throughout the cycles, indicating stability of the flow battery. Further, to have inexpensive, eco-friendly, and abundant material as an anolyte solution, Archana et al. [28], demonstrated the utilization of Fe-based couple, viz. Fe^{3+}/Fe^{2+}, along with Mn-based catholyte solution. However, the RFB showcases a decrease in the overall OCP due to the utilization of the Fe^{3+}/Fe^{2+} couple, and the theoretically obtained OCP corresponds to 0.79 V, viz. 1.5 V–0.77 V. In spite of a low OCP, the redox couples showcased an appreciable rate kinetics, and a high reversibility in their redox reactions, which can be visualized from the cyclic voltammetry graphs presented in the corresponding article [28].

Further, the flow battery has been discharged at various current densities ranging from 6–10 mA cm^{-2} to assess its rate capabilities, and the battery showcased a stable performance at 7 mA cm^{-2} for 100 cycles with CE%, VE, and EE% corresponding to 95%, 72%, and 68% respectively. Additionally, manganese based salts such as, $MnCl_2$ (6.42 M), $MnSO_4$ (4.17 M), $Mn(CH_3COO)_2$ (2.78 M) [33], showcase an elevated solubility in aqueous solution, as opposed to vanadium-based salts. This increment in the solubility of redox active materials aids significantly in enhancing the overall energy density (*E*) of the flow battery, and the theoretical evaluation of the same is showcased in the equation below:

$$E = \frac{nFCV}{3600},$$

wherein *n*, *F*, *C*, and *V* represent the number of electrons transferred, Faraday's constant, concentration of the redox-active species, and cell voltage, respectively. It is evident that the energy density is inherently dependent on the concentration of the redox-active materials, which in turn depends on the solubility of the corresponding salt in the solvent, viz., an aqueous solution. The future works might include the reduction of MnO_2 disproportionation reaction along with incorporating various other redox couples such as Cr, Sn, Eu, Cd, Pd, with appropriate cost-effective non-fluorinated ion exchange membranes, which has not been performed yet.

3. Vanadium-Based RFBs

The vanadium RFB is the currently commercialized, and a leading contender in the field of RFB technology, primarily owing to its ability to exhibit various oxidation states ranging from +2 to +5, which allows it to be utilized as catholyte, and anolyte [29,35,39,42,44–56] in combination with each other, or separately with a different redox active species. This unique ability aids in minimizing the dominant issue posed by 'electrolyte mixing' during a membrane breakage scenario. However, the traditional VRFB setup exhibits a theoretical overall cell potential of 1.26 V, as stated in the earlier reactions, which limits the ability of the RFB to possess higher energy density. To overcome this issue and to create an RFB with a broader OCP, a variety of flow batteries have been developed by replacing the vanadium counterpart with different redox couples [45–47,52,53], however, as explained earlier, this leads to a significant problem of electrolyte mixing, which will be addressed in the upcoming

sections. The vanadium +5 to +4 transition possesses a high potential, viz. 1 V vs. SHE, which, when coupled with an anolyte with greater potential as compared to its counterpart, can theoretically enhance the overall OCP of RFB, and thereby enhance the energy density. In this regard, Ulaganathan et al. [53] synthesized a hybrid RFB comprising vanadium catholyte and a zinc anolyte utilizing $ZnBr_2$. The synthesized hybrid RFB demonstrated a theoretical OCP of 1.76 V, as opposed to 1.26 V with VRFBs. However, the hybrid RFB demonstrates two significant problems, namely, electrolyte mixing and zinc dendrite formation (due to the '0' oxidation state of zinc, viz. Zn^0, making it a hybrid RFB).

$$2\ VO_2^+ + 4H^+ + Zn^0 \leftrightarrow 2\ VO^{2+} + Zn^{2+} + 2H_2O \quad E^0 = 1.76\ V$$
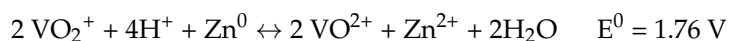
The synthesized hybrid RFB demonstrated a theoretical energy density of 559.68 Wh kg^{-1}, and the performance metrics have been compared with a separator and Nafion 117 at various discharging currents ranging from 10 to 50 mA cm^{-2}. The system showcased a CE%, VE%, and EE% of 83%, 84%, and 71%, respectively, at a discharge current density of 20 mA cm^{-2}. The use of a microporous separator caused vanadium-ion crossover, leading to self-discharge of the RFB and thereby reducing the overall energy storage capacity. The Zn-V hybrid RFB demonstrates high voltage, superior energy and power density, and better safety than the traditional hybrid Zn–Br systems. Its performance suggests it could replace conventional flow batteries for grid-scale renewable energy storage. However, the potential challenges, such as vanadium crossover, bromine side reactions, membrane cost, and moderate energy efficiency, must be resolved. The future research can be focused on developing advanced membranes to minimize crossover and self-discharge.

In a similar vein, the vanadium anolyte has been replaced with a chromium-based one to enhance the overall OCP of the VCRFB, and thereby to enhance the energy density. In this regard, Huo et al. [47] developed a vanadium-chromium RFB setup utilizing the higher redox potential of chromium, viz., 0.41 V vs. SHE (Cr^{2+}/Cr^{3+}), as an anolyte solution by utilizing $CrCl_3$ in various concentrations of H_2SO_4 and HCl solutions, while the catholyte has been synthesized by dissolving $VOSO_4$ in the same solution. The theoretical OCP of the VCRFB is 1.41 V, while it has been charged to 1.65 V in practical applications to overcome overpotentials and discharged at various current densities ranging from 40–160 mA cm^{-2} to assess its rate capabilities. Furthermore, to evaluate the stability of the flow battery, the VCRFB was discharged at a current density of 100 mA cm^{-2} for 50 cycles, wherein it displayed CE%, VE%, and EE% of 97%, 89%, and 87%, respectively. However, the VCRFB suffered from a significant capacity fade of 1.1% per cycle, which can be attributed to the crossover of the species through the membrane, leading to the self-discharge of the battery and the activation of HER. The future works on the VCRFB front can be focused on the development of a suitable ion exchange membrane, with lower permeabilities towards corresponding ions, while enhancing the ability of protons to be transferred to maintain the charge balance. Furthermore, to avoid the issue with mixing of the electrolyte during the operation of VCRFB, the electrolytes can be pre-mixed to evaluate their performance. The pre-mixing-based approach will be detailed in the upcoming section. Further, in order to reduce the price and utilize an abundant redox active material, Chen et al. [46] proposed a hybrid RFB utilizing vanadium-based catholyte (V^{4+}/V^{5+}), and Fe-based anolyte solution (Fe^{2+}/Fe^0). Replacing the vanadium anolyte (V^{3+}/V^{2+}) with an Fe-based couple, using ammonium iron (II) sulphate hexahydrate as the active species, and modifying the electrode, viz., a carbon paper, by depositing TiO2, and metal/alloy (Pd, or CoP) onto its surface, aided in the suppression of HER. Furthermore, the flow patterns have been modified, wherein serpentine and staggered patterns were utilized to enhance the electrolyte flow distribution across the electrode surface. The theoretical OCP of the resulting V–Fe RFB was 1.447 V, higher than that of commercialized VRFBs, leading to cost reduction. Moreover, to

evaluate the overall electrochemical performance of the V–Fe hybrid RFB, the battery was subjected to various discharge current densities ranging from 20–60 mA cm^{-2}, wherein the CE%, VE%, and EE% showcased appreciable values of greater than 95%, 71%, and 70%, respectively. However, the problem persisting with the V–Fe RFB is the depositing of Fe onto the surface of the electrode, which might lead to an issue of reduction in the overall capacity of the RFB due to a decrement in the available active species, and the imminent problem of excessive pressure build-up leading to damage to the RFB while pumping the liquid electrolyte. Although the V–Fe RFB holds the potential of being an interesting contender in the field of RFB technology, the long-term cyclic stability must be assessed prior to deployment. In contrast to the utilization of vanadium species as catholyte solution due to their high redox potential, it can be utilized as anolyte as well, when paired with a suitable high redox couple, such as Ce, which will be explored in the corresponding sections of the manuscript.

4. Iron-Based RFBs

Iron (Fe), being the 4th most abundant material available in the Earth's crust, while possessing a reasonably high redox potential of 0.77 V vs. SHE, portrays itself as a promising contender in the field of electrochemical storage devices, primarily RFBs. When compared to vanadium, manganese, or cerium, iron indeed has a lower redox potential; however, it is compensated by its extremely low cost and abundance as compared to the other materials, and acts as a potential redox-active species in an RFB system [14,28,44,49,55–65].

In the early 1970s, the iron-chromium RFB (ICRFB) was developed by NASA, which paved the path for future developments in the field of flow battery technology. Due to the low cost and abundance of the individual materials along with a reasonably high redox potential, viz., 0.77 V–Fe^{2+}/Fe^{3+} and 0.41-Cr^{2+}/Cr^{3+}, ICRFB stood out as a highly cost-effective large-scale energy storage device. Similar to the VRFBs, a typical ICRFB [14,56] setup consists of a carbon felt to soak up the liquid electrolyte, and acts as a site for the redox reactions to occur when placed adjacent to a graphite current collector plate through which the electrons travel. To maintain the charge balance across the anolyte and catholyte zones, an ion-exchange membrane has been deployed, which serves to separate the two electrodes within the battery and facilitates the necessary ion transport while preventing mixing of the electrolytes. The operation of an ICRFB generates a standard voltage of approximately 1.18 V, viz. 0.77 V + 0.41 V, achieved through a series of redox reactions between chromium and iron as shown below:

$$Fe^{2+} \leftrightarrow Fe^{3+} + e^- \qquad E^0 = 0.77 \text{ V vs. SHE,}$$

and

$$Cr^{2+} \leftrightarrow Cr^{3+} + e^- \qquad E^0 = -0.41 \text{ V vs. SHE.}$$

However, the ICRFB suffers from two significant issues, namely, the electrolyte mixing due to the presence of different ions in the catholyte and anolyte regions and a low OCP of 1.18 V (lower than a commercialized VRFB setup). In this regard, to evaluate the electrochemical performance of an ICRFB in comparison with an all-vanadium RFB setup, Zeng et al. [56] devised a study which utilizes the same battery setup and the volume of electrolyte, along with the concentrations, but differing in the redox active material. To evaluate the comparative behaviour of the VRFB and ICRFB, they were subjected to a range of current densities ranging from 40 to 160 mA cm^{-2} and cycled at a current density of 80 mA cm^{-2} to assess their long-term stability. The CE% of VRFB at the discharge currents ranging from 40–160 mA cm^{-2} ranged between 95% to 98%, whereas, for ICRFB it was in the range of 90% to 97%, suggesting a similar performance metric in regards to the CE%,

suggesting a minute ion crossover, and thereby self-discharging of the RFB. Furthermore, as per the cost analysis of the setup performed in the study, the ICRFB indicated a significant cost reduction in relation to the discharge duration and current densities as compared to a commercialized VRFB setup [56].

Further, in an effort to reduce the cost of RFBs consisting of iron-based catholyte, Kabtamu et al., [59] devised an iron-copper RFB comprising Cu-based anolyte. However, the redox potential of copper is 0.52 V vs. SHE, and the resulting Fe-Cu RFB demonstrated an OCP of 0.25 V, which is significantly lower compared to the currently commercialized VRFBs or ICRFBs or Mn-based RFBs. Although the RFB possess a minute OCP, the abundance of the active materials, and their toxicity is relatively negligible as compared to the commercialized ones, with an additional advantage of higher solubility of active materials in the aqueous solutions. This leads to an advantage of increasing the energy density, at the cost of an extremely low power density and OCP. Furthermore, to enhance the redox kinetics of Cu^{2+}/Cu^0 onto the electrode surface, Bi^{3+} has been deposited, which acts as a catalytic surface for the subsequent deposition and stripping of Cu. Moreover, the battery demonstrated a CE%, VE%, and EE% of 89%, 35%, and 39% at a discharge current density of 20 mA cm^{-2}. So, an optimum combination between the cost and working potential of the RFB must be stricken to advance the technology to a larger scale. Further, in order to enhance the OCP of the flow battery as opposed to utilizing a copper-based one, Chen et al., [44] devised an RFB consisting of vanadium-based anolyte (V^{2+}/V^{3+}) and Fe-based catholyte. The resulting flow battery demonstrated an OCP of 0.91 V, as opposed to the theoretical value of VRFB 1.26 V. In spite of possessing a lower OCP, the capital cost of the overall battery setup has been minimized by replacing iron as the catholyte instead of utilizing vanadium. The performance of the vanadium-iron RFB has been evaluated in comparison to VRFB, at various current densities ranging from 50–150 mA cm^{-2}, and their corresponding CE%, VE%, and EE% have been compared. The IVRFB showcased a CE% greater than 96% along the range of current densities, while the VE% dropped by approximately 10% as the discharge current density increased by 50 mA cm^{-2}. In this regard, the VRFB displayed an advantage by demonstrating a stable and minimal drop in the VE%, signifying a reduced ohmic resistance as compared to the IVRFB [44]. However, as mentioned earlier, the tradeoff between the cost and efficiency delivered at various current densities plays a crucial role in determining the RFB's ability to be deployed at the grid scale.

However, even after replacing the anolyte with vanadium, the low OCP still persists, causing a reduction in the energy density of the RFB setup. To overcome this issue, the anolyte has been replaced by zinc, which possesses a higher redox potential as opposed to V^{2+}/V^{3+}. In this regard, numerous studies have been performed, of which Chang et al. [57] utilized zinc as the anolyte and iron as the catholyte solutions along with a low-cost K^+ ion transfer SPEEK membrane to reduce the overall cost incurred due to the Nafion membrane on the RFB. The overall OCP of the demonstrated iron-zinc RFB showcased a value of approximately 1.5 V, due to the higher reduction potential of zinc, viz., 0.76 V vs. SHE–Zn^{2+}/Zn^0. The RFB has been discharged at current densities ranging from 10–60 mA cm^{-2}, and the Zn-Fe RFB showcased a CE%, VE, and EE% of greater than 95%, 78%, and 74% respectively, at a cost of 1/13th of Nafion, due to the utilization of SPEEK membrane. Further, the reduction potential of zinc raises when dissolved in an alkaline solution, and the same has been demonstrated by Gong et al. [58] The study utilizes a unique arrangement of the RFB setup to compensate for the utilization of acid/base system, wherein, the anolyte involves conversion of $Zn(OH)_4^{2-}$ to Zn in the presence of NaOH solution, and the catholyte utilizes the traditional Fe^{3+}/Fe^{2+} redox couple in HCl solution. Moreover, the anolyte and the catholyte chambers have been separated by a buffer region,

which consists of a neutral NaCl solution, aiding in the transport of ions by utilizing a cation (CEM) and an anion exchange membrane (AEM). The presence of a CEM at the $NaCl/Zn(OH)_4^{2-}$ interface aids in the transport of Na^+ ions through it, and the AEM at the interface of Fe/NaCl transports the chloride ions, maintaining a charge balance while the electrons travel through the outer circuit. The construction is as shown in Figure 2. This unique assembly of the RFB setup, along with utilizing the high reduction of zinc in the presence of an alkaline medium, overall OCP of the Zn-Fe RFB reached 1.99 V, aiding significantly in enhancing the energy density.
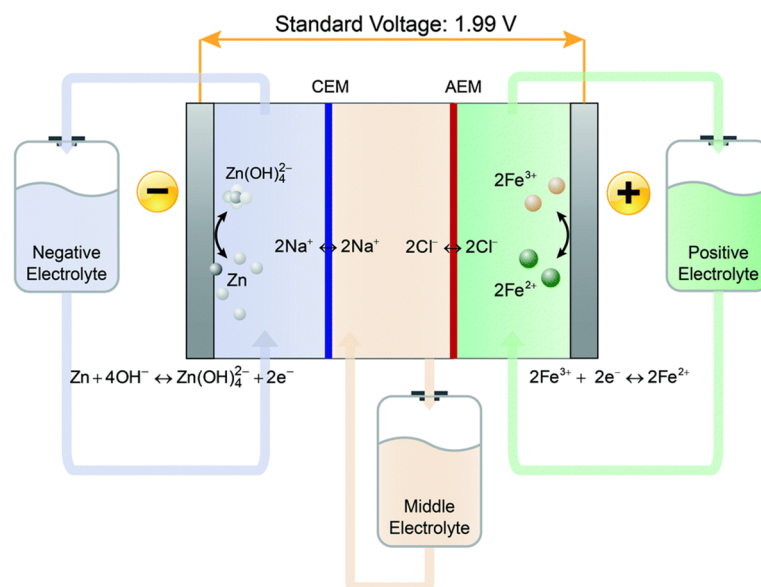

Figure 2. The schematic of a hybrid zinc iron redox flow battery utilizing two different compartments along with their respective membranes, wherein $Zn(OH)_4^{2-}$ is utilized as the anolyte solution, and an iron-based catholyte solution [58].

Furthermore, the battery showcased a stable CE%, VE%, and EE% of 99.9%, 76.0%, and 75.9% at a discharge current density of 80 mA cm^{-2} for numerous cycles. However, the main problem that arises with the utilization of Zn-based RFB is the electroplating, i.e., deposition of Zn^0 onto the surface of the electrode, leading to a growth of dendrite, and thereby reducing the overall energy density of the flow battery as the cycles progress.

In similar lines of utilizing new anolytes in combination with Fe-based catholyte, Zeng et al. [63] presented a novel hybrid RFB comprising lead as the anolyte, viz., Pb/Pb(II), due to its abundance, and iron as the catholyte solution, viz. Fe(II)/Fe(III), resulting in a reduction in the system's overall cost. The resulting RFB setup showcased an OCP of 0.9 V, which is significantly lower compared to the Zn–Fe RFB comparison of alkaline solution. To enhance the electrode kinetics, an organic acid has been utilized, viz., methanesulfonic acid (MSA). The utilization of MSA aided in enhancing the ionic conductivity and the solubility of Pb and Fe in the aqueous solution. Furthermore, to avoid the problem arising due to the cross-mixing of the electrolytes, the author devised a pre-mixed electrolyte approach. Prior to the initialization of the RFB, the synthesized electrolytes consisting of Fe and Pb have been pre-mixed at 0% SOC, and divided into equal volumes to be further utilized as catholyte and anolyte solutions. The resulting RFB showcased a CE% of 96.2%, and 98.2% at discharge current densities of 40 mA cm^{-2}, and 120 mA cm^{-2}, with an EE% of 86.2%, and 73.5% respectively at similar currents. In similar lines of pre-mixing the electrolytes at 0% SOC, prior to the charge-discharge studies of the RFB, the same author utilized a different combination of anolyte and catholyte solutions comprising cadmium and iron, respectively [62]. The reduction potential of Cd^{2+}/Cd^0 is 0.4 V, which is higher than the

reduction potential of V^{2+}/V^{3+}; however, the usage of cadmium poses severe environmental threats, and extremely careful precautions must be followed. Prior to developing a flow battery, the authors utilized a static cell, wherein 80 μL of the electrolytes was utilized in a stationary, and non-flow format cell, to evaluate the electrochemical characteristics at a discharging current density of 15 mA cm^{-2}. Further, a hybrid Fe-Cd RFB was utilized by incorporating a zero-gap flow-through cell structure to evaluate its behaviour under continuous flow conditions. The hybrid RFB showcased an impressive performance by demonstrating a CE%, and EE% of 98.7%, and 80.2% at a discharge current density of 120 mA cm^{-2} [62]. Furthermore, the hybrid RFB exhibited stable cyclic charge-discharge performance, with a capacity retention of 99.87%.

The main aim of including the following studies is to highlight the ability to mitigate the crossover problem in spite of utilizing different anolytes and catholytes, by following a pre-mixed electrolyte method. Of the various types of RFBs currently being studied in regards to the Fe-based catholyte, Zn-Fe RFB showcased an appreciable OCP of 1.99 V [58], owing to the ability of zinc, which has demonstrated a high reduction potential in a basic solution. This concept can be extrapolated to various couples consisting of a higher reduction potential, and acting as catholyte, such as vanadium (1.0 V vs. SHE), cerium (1.61 V vs. SHE), manganese (1.5 V vs. SHE), and bromine (1.08 V vs. SHE).

5. Cerium-Based RFBs

Among the various rare earth elements available in the earth's crust, cerium (Ce) holds the highest position in abundance, making it a viable alternative to be utilized as a potential redox-active material for the RFB technology. Along with its abundance, cerium has a high reduction potential, viz. Ce^{3+}/Ce^{4+}–1.61 V vs. SHE, making it a suitable candidate to be utilized as a catholyte in Ce-based RFBs [48,66–77]. Due to its high redox potential, it can be paired with almost any anolyte combination, such as vanadium, zinc, polysulphides, lead, europium, chromium, and demonstrate a high OCP as compared to a commercialized VRFB technology. In this regard, Na et al., [70] developed a hybrid RFB consisting of Ce-based catholyte (Ce^{3+}/Ce^{4+}), and Pb-based anolyte (Pb^{2+}/Pb^{0}), owing to their low cost, and abundance of the redox active materials. Cerium(III) carbonate and lead (II) oxide were dissolved in MSA and DI water, wherein MSA acts as a supporting electrolyte owing to its high ionic conductivity, low corrosivity, and its ability to enhance the solubility of Pb and Ce, which aids in increasing the energy density of the hybrid Ce-Pb RFB. The proposed RFB demonstrated a theoretical OCP of approximately 1.74 V (depending on the concentrations of the individual redox active material), which is higher than several other RFBs, such as VRFBs, ICRFBs, V-Zn RFBs, V–Fe RFBs, Mn-V RFBs, Mn-Ti RFBs. Furthermore, due to the high overpotential of Pb-based anolyte, it inhibits the hydrogen evolution reactions occurring at the surface of the anode. To assess the electrochemical performance, various discharging currents have been provided, ranging from 2.5 mA cm^{-2} to 10 mA cm^{-2}, and the hybrid Ce-Pb RFB showcased a CE% of greater than 95%, and an EE% higher than 70%. Furthermore, to evaluate the stability of the flow battery, a discharging current of 5 mA cm^{-2} has been utilized for over 800 cycles of operation, wherein the RFB showcased a CE% and EE% greater than 90% and 80% respectively [70].

It has been demonstrated that the RFB possesses high efficiency and stability across numerous cycles of operation over a wide temperature range. However, as mentioned earlier, the deposition of Pb^{0} onto the electrode surface might reduce the overall energy storage capacity of the Ce–Pb RFB and requires an in-depth analysis of the same, as the technology is currently in the proof-of-concept stage but holds potential to be commercialized. In similar lines of enhancing the OCP, Leung et al. [48] presented a vanadium–cerium RFB utilizing vanadium (V^{2+}/V^{3+}) as the anolyte, and cerium as catholyte solutions, along with

a zero-gap serpentine flow field to reduce the internal resistance, enhance mass transport, and eventually achieve a higher energy density. The presented V-Ce RFB showcases a theoretical OCP in the range of 1.54 V to 1.98 V, depending on the concentrations of the individual redox active species in the electrolyte region. Vanadium aids in enhancing the overall energy density of the RFB due to its ability to be dissolved in higher concentrations, viz., greater than 2 M; however, the solubility of Ce is comparatively lower, leading to the utilization of a mixed-acid supporting electrolyte setup, viz., MSA + H_2SO_4 in a 3:1 ratio. The RFB setup has been subjected to a current density of 100 mA cm^{-2} till it reaches a capacity of 650 mAh, suggesting an 80% SOC. The RFB showcased a CE% of 94%, compared to 89% for a conventional non-zero-gap serpentine structure, and a power density of 370 mW cm^{-2}, a two-fold increase over the traditional one. Furthermore, the RFB showcased an energy density of 28 Wh L^{-1} which is comparable with VRFBs (20–30 Wh L^{-1}), but with a higher OCP of approximately 1.78 V.

In these similar lines, Wu et al., [75] developed an RFB by utilizing a rather new anolyte combination, viz., europium (Eu), which has a standard reduction potential of 0.35 V vs. SHE during the reduction of Eu^{3+} to Eu^{2+}. The developed Eu-Ce RFB showcased a theoretical OCP of 1.96 V and non-toxic characteristics, and the battery demonstrated an energy and power density of 43 Wh L^{-1} and 484 mW cm^{-2}, respectively. This is an approximate two-fold increase compared to traditional VRFBs dissolved in MSA, to enhance the solubility of the redox-active species, viz., 1 M and 1.2 M for Ce and Eu, respectively. Over 100 stable cycles at 100 mA cm^{-2}, it demonstrated an outstanding CE% of 98%, VE of 84%, and EE% of 82.4%, with a high average discharge voltage of 1.81 V [75]. The study also shows that increasing active species concentration improves CE% by suppressing the side reactions, viz. HER, while slightly reducing VE due to concentration polarization.

The utilization of Eu has indeed proved to be a notable RFB system comprising rare earth materials with lower toxicity and higher reduction potentials. However, the long-term cyclic stability of the proposed RFB still remains a question, which can be addressed as a potential path for the upcoming research at various temperatures and current densities. Furthermore, as per the literature survey, the utilization of Eu has been restricted primarily to Ce-based RFBs, which can be extrapolated to a whole new array of redox-active species to potentially serve as an energy storage device. While the Eu–Ce system demonstrated an exceptional electrochemical performance with an OCP of 1.96 V, it should be noted that europium is one of the rarest and expensive rare-earth elements, with an average abundance of only 1–2 ppm in the Earth's crust, along with a limited global production. Although the Eu–Ce chemistry is scientifically significant as a high-voltage aqueous flow battery system, it is highly unlikely to be viable for grid-scale energy storage. Rather, this study can be utilized as a primary source to illustrate the rare-earth-based redox couples, to derive insightful thoughts that can be extrapolated to an abundant system for high voltage applications.

Further, to reduce the cost of active species, along with enhancing the OCP, similar to several other studies, Silambarasan et al. [74] utilized polysulphide-based anolyte solution, and Ce-based catholyte. The study utilized an acid-base system and a single MFI-Zeolite membrane separator to achieve high energy densities as compared to the other RFBs. The term 'MFI' refers to a zeolite framework structure first developed by Mobil Corporation, and it is represented by the well-known ZSM-5 zeolite. This framework contains a three-dimensional network of 10-membered oxygen-ring channels with pore sizes of about 0.54–0.56 nm to selectively allow proton conduction while blocking the crossover of larger hydrated ions. This molecular sieving property of MFI-zeolite membrane aids in reducing the self-discharge characteristics of the flow battery, and thereby enhancing the CE%. The system leverages the wide potential window created by combining an acidic Ce^{3+}/Ce^{4+}

half-cell (1.61 V vs. SHE) with a basic polysulfide $S_4^{2-}/2S_2^{2-}$ anolyte (0.45 V vs. SHE), theoretically yielding a total cell potential of 2.06 V, depending on the concentrations of the species, which is significantly higher than conventional VRFBs (1.26 V). The MFI-Zeolite membrane is crucial because its 0.56 nm pore size allows proton transfer while preventing the crossover of bulky hydrated cerium and sulphur ions, addressing a common issue faced in the RFBs. UV-VIS studies showed no detectable migration of Ce^{3+} or S_4^{2-} over 500 h, confirming the effectiveness of the MFI-Zeolite membrane. The Ce-S system achieved a current efficiency of 94% and an excellent energy density of 378.3 Wh L^{-1}, far exceeding typical values for aqueous RFBs. At a current density of 10 mA cm^{-2}, the battery delivered voltage and energy efficiencies of 40–43%, which needs to be further investigated to fully unlock the potential of Ce-S RFB. Despite these promising results, challenges remain, including the relatively low voltage efficiency due to the large open-circuit potential difference caused by the acid-base configuration. Overall, this work demonstrates a viable strategy to dramatically boost aqueous RFB energy density by combining pH-differentiated electrolytes with a highly selective, low-cost zeolite membrane.

Further, the well-known and extensively researched Ce-based RFBs consist of utilizing zinc as anolyte, due to its high reduction potential, viz., 0.76 V vs. SHE (Zn^{2+}/Zn^0), abundance and low cost of active materials. Numerous studies have been performed in this regard to study the life cycle analysis of the flow battery, efficiency variation at various temperatures, current densities, stability, etc. In this regard, Amini et al., [66] explores an effective strategy to improve the performance of zinc–cerium hybrid redox flow batteries (Zn–Ce hybrid RFBs) through the use of a mixed MSA-chloride negative electrolyte instead of the conventional pure MSA-based electrolyte. Zn–Ce hybrid RFBs are a potential candidate for large-scale energy storage because of their extremely high OCP of 2.4 V, which provides higher energy density and power output compared to conventional VRFBs. However, their commercialization has been hindered by several challenges, of which HER at the negative electrode and zinc deposition play a crucial role in advancing the Zn-Ce RFB. Rather than irregular zinc deposition on the electrode surface (dendrite growth), a uniform deposition is essential to ensure long-term stability for Zn-based RFBs. In this preface, the study builds on previous work that proved that chloride ions can significantly improve zinc deposition by lowering the nucleation overpotential (NOP) and enhancing electron transfer through adsorption at the electrode surface, rather than a non-uniform or localized deposition leading to dendrite formation.

The electrochemical tests performed on the modified Zn-Ce RFB showcased that, when the mixed MSA–chloride$^-$ electrolyte was used, the VE% increased from 60% to 66% at a current density of 25 mA cm^{-2}, while the CE% remained initially unchanged due to the cerium redox reaction being the limiting factor during the first cycle. However, when the cerium half-cell was initially pre-charged to remove this limitation, the CE% rose significantly from 64% to 81%, showing that the presence of chloride ions dramatically improves the zinc-side performance by ensuring a uniform deposition of Zn^{2+} ions onto the electrode surface. Extended cycling revealed that with the mixed electrolyte, zinc deposition was more stable, leading to longer discharge times.

At different current densities ranging from 15 mA cm^{-2} to 30 mA cm^{-2}, the advantages of the mixed electrolyte were even more pronounced. At a lower current density, the CE% increased from 54% to 73%, while at a higher current density, the CE% rose from 58% to 80%, indicating the chloride ions effectively suppressed side reactions (HER). Furthermore, the life-cycle analysis showed a dramatic 70% increase in operational life: the battery using the conventional electrolyte lasted for 42 h and 97 cycles, whereas the one with the mixed electrolyte operated for over 75 h and 166 cycles under identical conditions. These studies

illustrate the advantages of utilizing cerium as a potential catholyte alternative, owing to its high standard reduction potential and redox capabilities.

6. Halide-Based RFBs

Halides such as bromide and iodide exhibit highly reversible redox kinetics, along with an ability to be dissolved in aqueous solutions to a larger extent, allowing for a possible enhancement in the overall energy density of the halide-based RFB setup [13,51,54,78–84]. However, despite their advantages, they do pose a few challenges, such as high corrosivity and volatility, leading to electrolyte loss, material degradation, and thereby negatively impacting the long-term cyclic stability of the halide-based RFB setup. In this regard, Li et al., [79] developed a halide-based RFB utilizing ZnI_2 (highly soluble salt, viz., approximately till 7 M), wherein Zn acts as the anolyte solution, and iodine as the catholyte, as shown in Figure 3a. The theoretical overall OCP of the hybrid Zn-I RFB can be calculated based on their individual standard reduction potential, viz., $I_3{}^-/I^-$ (0.53 V vs. SHE), and Zn^{2+}/Zn^0 (0.76 V vs. SHE), leading to RFB exhibiting 1.29 V, which is comparable to VRFBs at a reduced material cost, and increased abundance of the redox active materials.
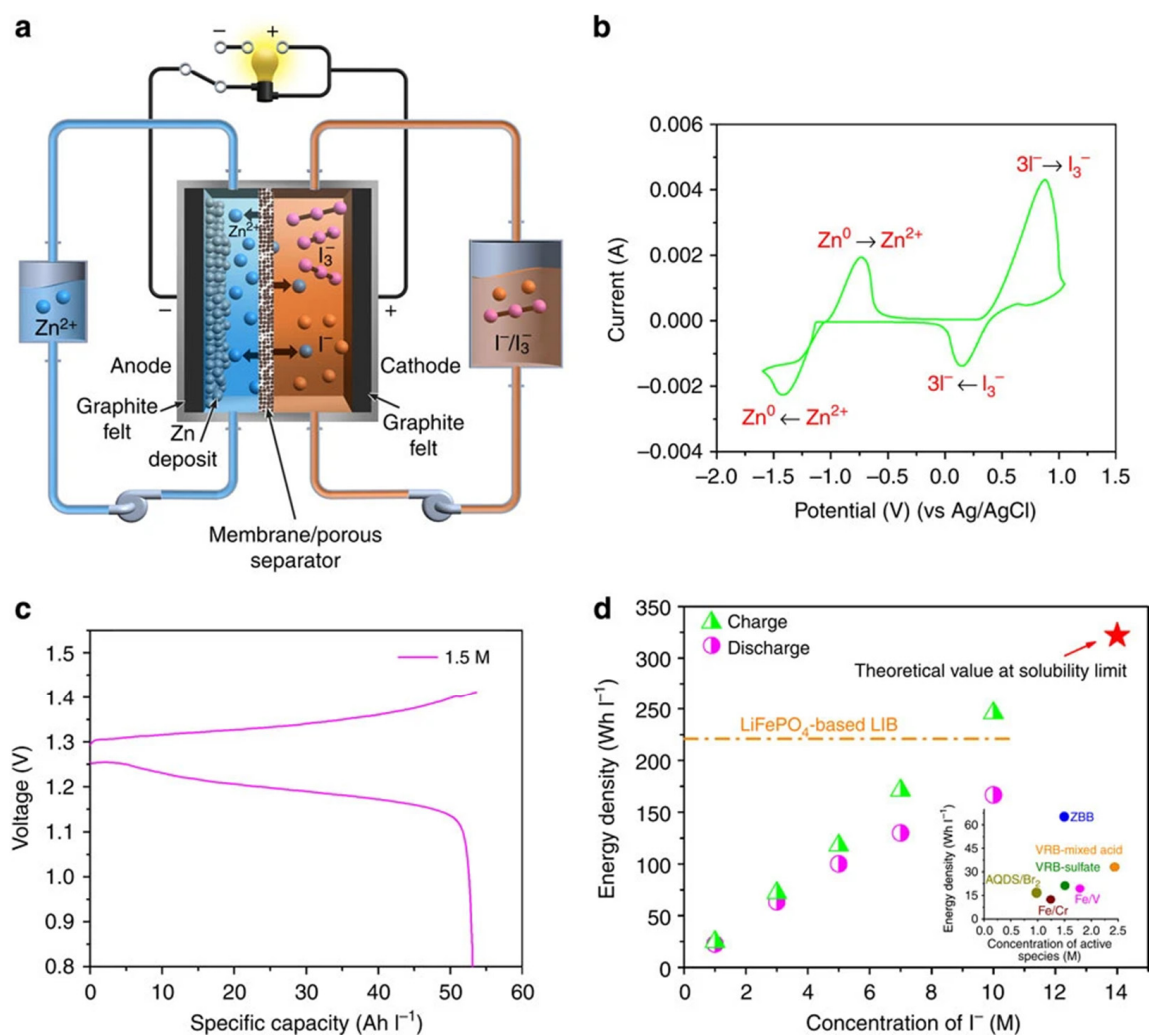

Figure 3. A working prototype's schematic of the hybrid zinc-iodide redox flow battery (**a**); Cyclic voltammetry measurements of 0.085 M ZnI_2 on a glassy carbon electrode performed at a scan rate of 50 mV s^{-1} (**b**); the charge-discharge profile of a single cycle for an electrolyte comprising 1.5 M ZnI_2, measured at a discharging current density of 20 mA cm^{-2} (**c**); the variation in the energy density of the hybrid Zn-I redox flow battery measured as a function of concentration of I^- (**d**) [79].

The theoretical energy density of a hybrid Zn-I RFB can potentially reach up to 322 Wh L^{-1} at a concentration of 14 M (ZnI_2 in DI water), calculated based on the catholyte solution, due to the electroplating of anolyte, i.e., Zn, onto the electrode surface. Further, the RFB has been subjected to a discharge current of 10 mA cm^{-2} at various temperatures ranging from $-20\,°C$ to $25\,°C$, and the CE% remained well over 95%, with a varying VE% in the range of 55% to 85% due to the increase in the ohmic drops, primarily as a result of enhanced mass transport resistance due to the increased viscosity, and reduced solubility leading to the precipitate formation, as the temperature decreases. A long-term cyclic stability test can indeed be essential to evaluate its impact at various temperatures and current densities to unlock the full potential of Zn-I RFBs.

In similar lines of utilizing zinc as anolyte, several studies have been published by incorporating bromide-based catholyte solution, as it is regarded as a potential candidate in the large-scale energy storage solution. Following this, Zhang et al., [84] developed a carbon-coated microporous membrane to reduce the internal resistance, and thereby aid in enhancing the overall efficiency of the RFB, and the power densities as opposed to its lower values in the previously developed hybrid Zn-Br RFBs. The overall OCP of the cell has been demonstrated to be approximately 1.83 V, signifying the high reduction potential of bromide (Br^-/Br_2) based catholyte, viz. 1.07 V vs. SHE. Further, the performance of the RFB has been evaluated at 20 mA cm^{-2} and 40 mA cm^{-2}, wherein the hybrid Zn-Br RFB showcased EE%'s of 73.2, and 44.6% for the conventional separator, while the CCM separator demonstrated 80.3% and 75.0% respectively, signifying the improvement in the electrochemical performance. However, the long-term cyclic stability of the hybrid Zn-Br RFB utilizing the modified membranes remains a question that can be further investigated to aid successful large-scale deployment. In similar lines of utilizing inexpensive catholyte and anolyte materials while retaining a high OCP and efficiencies of the halide-based RFBs, polysulfides have been incorporated by numerous researchers, due to their high standard reduction potential of approximately 0.54 V vs. SHE (depending on the concentrations), and low material procurement costs. Furthermore, as illustrated in the earlier sections, the utilization of an acid-based system, i.e., an alkaline solution of Na or K polysulfides, in comparison with a neutral or acidic system, can aid in enhancing the overall OCP of the flow battery. In this regard, Li et al., [43] demonstrated a polysulfide–iodide RFB (PSIRFB), and performed operando UV-VIS spectroscopy to investigate the intermediates formation during the reaction, and thereby obtain an in-depth understanding of the PSIRFB. However, the RFB suffers from a low OCP of approximately 1.05 V, depending on the concentrations of the redox-active species, compared to commercialized VRFBs, but excels at minimizing the cost of procuring redox-active materials. Furthermore, due to the high solubility of polysulfides and iodides (greater than 5 M), this leads to a significant enhancement in the overall energy density, viz., 43.1 Wh L^{-1} (catholyte+anolyte). Moreover, the peak separations of I^-/I_3^- (0.17 V), and S^{2-}/S_2^{2-} (0.28 V) at 20 mV s^{-1}, is lower as compared to vanadium or bromide catholyte redox reactions, signifying improved redox kinetics. Furthermore, the operando UV-VIS performed in the study plays a crucial role in determining the oxidation states of iodine and polysulfides during the oxidation and reduction processes occurring at various potentials. Due to the complex nature of polysulfides, it is indeed necessary to understand their behaviour under varying voltages, to determine the presence of short and long-chained polysulfides [43].

Due to the incorporation of inexpensive anolyte and catholyte materials, the material cost per kilowatt hour reduces from approximately \$154.6 kW h^{-1} to \$85.4 kW h^{-1}, by maintaining a CE% greater than 90% at various discharge current densities ranging from 5–25 mA cm^{-2}, signifying its potential to be utilized as an RFB in large-scale energy storage. In these similar lines, rather than utilizing iodine, bromide has been incorporated

as the catholyte solution by numerous researchers dating from the late 90s, due to its higher standard reduction potential of 1.07 V vs. SHE, resulting in a RFB with an OCP of approximately 1.54 V. Of these, Zhao et al., [13] utilized a nickel foam treated in Na_2S_4 to form NiS_x, as the negative electrode, and carbon felt as the positive one, to aid in the redox kinetics of the polysulfide-bromide RFB system, which has later been utilized by numerous studies while developing RFBs consisting of polysulfides as the anolyte solution. The results showcased that nickel foam displays a very low overpotential for polysulfide reactions (≤ 27 mV at 50 mA cm^{-2}), along with the highest EE% of 77.2% at 40 mA cm^{-2}, and an average CE%, VE%, and EE% of greater than 90%, 80%, and 75% respectively. To conclude, based on the review of literature regarding the various inorganic and hybrid redox flow battery chemistries, a table has been formulated as showcased in Table 1, summarizing the reduction potentials, abundancies, efficiencies, toxicities, and their respective half-cell reactions.

Table 1. A comparative summary of major inorganic aqueous and hybrid redox flow battery chemistries, along with their key electrochemical and material characteristics. Here, RFB denotes a redox flow battery, and HFB represents the hybrid flow battery.

System/ Redox Pair	Half-Cell Reaction	Open Circuit Potential	Type	Toxicity	Elemental Abundance	Typical CE/EE (%)	Remarks
$V^{5+}/V^{4+}-$ V^{2+}/V^{3+}	$VO_2^+ + 2H^+ + e^-$ $\rightleftharpoons VO^{2+} + H_2O$; $V^{3+} + e^- \rightleftharpoons V^{2+}$	1.26	RFB	Moderate (acidic corrosion– H_2SO_4)	Abundant (0.012 wt% crustal)	95–99%/70–80%	Benchmark system; limited by cost volatility, solubility, and corrosive properties.
$Ce^{4+}/Ce^{3+}-$ Pb^{2+}/Pb^0	$Ce^{4+} + e^- \rightleftharpoons Ce^{3+}$; $Pb^{2+} + 2e^- \rightleftharpoons Pb^0$	1.74	HFB	Pb is toxic	Ce-moderately abundant (0.006% wt% crustal); Pb-moderately abundant (0.0014% wt% crustal)	95%/70%	High voltage; HER suppressed by Pb deposition. Low solubility of cerium-based salts.
$Ce^{4+}/Ce^{3+}-$ S_x^{2-}/S_2^{2-}	$Ce^{4+} + e^- \rightleftharpoons Ce^{3+}$; $S_x^{2-} + 2e^- \rightleftharpoons xS^{2-}$	2.06	RFB	Low toxicity	Ce-moderately abundant (0.006% wt% crustal); S-abundant (0.04% wt% crustal)	94%/43%	High potential of Ce; Acid–base hybrid; crossover mitigated by MFI membrane.
$Fe^{3+}/Fe^{2+}-$ Cr^{3+}/Cr^{2+}	$Fe^{3+} + e^- \rightleftharpoons Fe^{2+}$; $Cr^{3+} + e^- \rightleftharpoons Cr^{2+}$	1.18	RFB	Low toxicity	Fe-extremely abundant (5.0% wt% crustal); Cr-abundant (0.01 wt% crustal)	90–97%/70–80%	Cost-effective; HER major side reaction at the Cr side.
$Mn^{3+}/Mn^{2+}-$ Ti^{4+}/Ti^{3+}	$Mn^{3+} + e^- \rightleftharpoons$ Mn^{2+}; $Ti^{4+} + e^- \rightleftharpoons Ti^{3+}$	1.55	RFB	Low toxicity	Mn-abundant (0.1% wt% crustal); Ti-abundant (0.63% wt% crustal)	99.8%/86.7%	High potential; Mn^{3+} disproportionation mitigated by Ti complexation. Mixed electrolyte preferred.
Zn^{2+}/Zn^0- Br_2/Br^-	$Zn^{2+} + 2e^- \rightleftharpoons Zn^0$; $Br_2 + 2e^- \rightleftharpoons 2Br^-$	1.83	HFB	Moderate (Br volatility)	Zn-moderately abundant (0.0075% wt% crustal); Br-moderately abundant (2.5 ppm–crustal, 67 ppm–ocean water)	98%/70–80%	High energy density; High solubility of halides; Risk of Zn dendrite growth, Bromine gas evolution.

Table 1. *Cont.*

System/ Redox Pair	Half-Cell Reaction	Open Circuit Potential	Type	Toxicity	Elemental Abundance	Typical CE/EE (%)	Remarks
Zn^{2+}/Zn^0– I_3^-/I^-	$Zn^{2+} + 2e^- \rightleftharpoons Zn^0$; $I_3^- + 2e^- \rightleftharpoons 3I^-$	1.29	HFB	Moderate toxicity	Zn-moderately abundant (0.0075% wt% crustal); I-moderately abundant (0.5 ppm–crustal, 0.05 ppm–ocean water)	95%/75–85%	Stable; High solubility of halides; Comparatively safer hybrid; Zn dendrite growth.
Fe^{3+}/Fe^{2+}– Cd^{2+}/Cd^0	$Fe^{3+} + e^- \rightleftharpoons Fe^{2+}$; $Cd^{2+} + 2e^- \rightleftharpoons Cd^0$	1.27	HFB	Cd highly toxic	Fe-extremely abundant (5.0% wt% crustal); Cd-extremely scarce (0.1 ppm–crustal)	98%/80%	Extreme toxicity; Higher OCP than VRFBs; Low cost battery; Cadmium deposition (Cd^0); Proof-of-concept only.
Eu^{3+}/Eu^{2+}– Ce^{4+}/Ce^{3+}	$Eu^{3+} + e^- \rightleftharpoons Eu^{2+}$; $Ce^{4+} + e^- \rightleftharpoons Ce^{3+}$	1.96	RFB	Low toxicity	Ce-moderately abundant (0.006% wt% crustal); Eu-extremely scarce (0.00018% wt% crustal)	98%/80% –85%	High OCP; Impractical due to Eu being the rarest rare earth metal; Scarcity & cost.
S_x^{2-}/S_2^{2-}– I_3^-/I^-	$S_x^{2-} + 2e^- \rightleftharpoons xS^{2-}$; $I_3^- + 2e^- \rightleftharpoons 3I^-$	0.90–1.20	RFB	Moderate toxicity	S-abundant (0.04% wt% crustal); I-moderately abundant (0.5 ppm–crustal, 0.05 ppm–ocean water)	90%/70%	High solubility; Good reversibility; Low cost; low OCP as compared to VRFBs.

7. Conclusions

This comprehensive review demonstrates that moving beyond a single redox-active material paradigm, and diversifying the redox chemistries through the exploration of various component combinations of inorganic redox-active species, offers a viable route to overcome the inherent voltage and cost limitations of conventional VRFBs. By pairing high-potential catholytes such as Ce, Fe, Mn, and halides with various compatible anolytes, including Ti, Zn, Pb, Cr, polysulfides, and rare earth elements, several studies have achieved higher OCPs and enhanced energy efficiencies while reducing the system costs. The reduction in cost, along with improved energy density, efficiency, and OCPs, significantly aids the deployment of the RFB at the grid scale. As per the review, the availability of anolytes with high reduction potentials is rather limited compared to that of catholytes. This issue can be addressed by the incorporation of rare earth elements, due to their extremely high reduction potentials; however, they showcase limited stability across various oxidation states, resulting in self-discharge in the RFB.

In the short term, iron, zinc, and manganese-based hybrid systems are the most promising candidates for commercialization. Their combination of high abundance, low toxicity, and electrochemical stability, particularly in Fe–Zn, Mn–Ti, Mn-Zn, and Zn–Br/I solution, allows for a scalable and cost-effective energy storage solution with OCPs voltages exceeding 1.5 V, while offering a higher solubility as compared to vanadium. These systems can be integrated into existing flow-battery infrastructure with relatively minor material and engineering modifications. In contrast, cerium and halide-based chemistries exhibit exceptional energy densities and voltages (up to 2.0 V) but require further optimization in electrolyte formulation. However, the limited solubility of cerium-based salts limits the broadening of their energy density. This issue can be addressed by the incorporation of ionic liquids to enhance the solubility and thereby the energy density.

Meanwhile, rare-earth systems (Eu–Ce), though scientifically significant for advancing the inorganic high-voltage RFBs, remain impractical for commercial application due to their scarcity and cost.

The pathway to translating these chemistries into commercial devices will depend not only on the redox pairs but also on component-level advances that mitigate inherent chemical challenges. Next-generation, cost-effective and selective ion-exchange membranes, including sulfonated poly(ether ether ketone) (SPEEK), zeolite, and composite membranes, can aid in reducing the ionic crossover while maintaining proton conductivity. On the electrolyte side, complexing agents, acid-base systems, and the incorporation of nanofluids can stabilize high-valence species and reduce their inherent precipitation or gas evolution.

In summary, the continued evolution of chemistry design and materials engineering will be essential for advancing inorganic aqueous and hybrid redox flow batteries from laboratory prototypes toward grid-scale commercialization. Systems that effectively provide high voltage, stability, low cost, and sustainability, supported by robust membrane and electrode engineering, are destined to define the next generation of high-performance, long-life, and economically viable flow batteries.

Author Contributions: Y.Z.—Conceptualization, methodology, writing—review, supervision, project administration, funding acquisition. C.K.S.K.—Methodology, writing—original draft, writing—review and editing, data curation. All authors have read and agreed to the published version of the manuscript.

Data Availability Statement: No new data was created or analyzed in this study. Data sharing is not applicable to this review article.

Conflicts of Interest: The authors declare no conflicts of interest.

References

1. Winter, M.; Brodd, R.J. What are batteries, fuel cells, and supercapacitors? *Chem. Rev.* **2004**, *104*, 4245–4269. [CrossRef] [PubMed]
2. Steele, B.C.H.; Heinzel, A. Materials for fuel-cell technologies. *Nature* **2001**, *414*, 345–352. [CrossRef]
3. Yabuuchi, N.; Kubota, K.; Dahbi, M.; Komaba, S. Research development on sodium-ion batteries. *Chem. Rev.* **2014**, *114*, 11636–11682. [CrossRef] [PubMed]
4. Nitta, N.; Wu, F.; Lee, J.T.; Yushin, G. Li-ion battery materials: Present and future. *Mater. Today* **2015**, *18*, 252–264. [CrossRef]
5. Goodenough, J.B.; Park, K.S. The Li-ion rechargeable battery: A perspective. *J. Am. Chem. Soc.* **2013**, *135*, 1167–1176. [CrossRef]
6. Dunn, B.; Kamath, H.; Tarascon, J.M. Electrical energy storage for the grid: A battery of choices. *Science* **2011**, *334*, 928–935. [CrossRef]
7. Goodenough, J.B.; Kim, Y. Challenges for rechargeable Li batteries. *Chem. Mater.* **2010**, *22*, 587–603. [CrossRef]
8. Conway, B.E. Transition from "Supercapacitor" to "Battery" Behavior in Electrochemical Energy Storage. *J. Electrochem. Soc.* **1991**, *138*, 1539–1548. [CrossRef]
9. González, A.; Goikolea, E.; Barrena, J.A.; Mysyk, R. Review on supercapacitors: Technologies and materials. *Renew. Sustain. Energy Rev.* **2016**, *58*, 1189–1206. [CrossRef]
10. Liu, C.; Li, F.; Lai-Peng, M.; Cheng, H.M. Advanced materials for energy storage. *Adv. Mater.* **2010**, *22*, E28–E62. [CrossRef] [PubMed]
11. Simon, P.; Gogotsi, Y.; Dunn, B. Where do batteries end and supercapacitors begin? *Science* **2014**, *343*, 1210–1211. [CrossRef]
12. Chivukula, K.S.K.; Zhao, Y. Next-generation vanadium redox flow batteries: Harnessing ionic liquids for enhanced performance. *RSC Adv.* **2025**, *15*, 25310–25321. [CrossRef]
13. Zhao, P.; Zhang, H.; Zhou, H.; Yi, B. Nickel foam and carbon felt applications for sodium polysulfide/bromine redox flow battery electrodes. *Electrochim. Acta* **2005**, *51*, 1091–1098. [CrossRef]
14. Zeng, Y.K.; Zhou, X.L.; An, L.; Wei, L.; Zhao, T.S. A high-performance flow-field structured iron-chromium redox flow battery. *J. Power Sources* **2016**, *324*, 738–744. [CrossRef]
15. Kosswattaarachchi, A.M.; Cook, T.R. Concentration-dependent charge-discharge characteristics of non-aqueous redox flow battery electrolyte combinations. *Electrochim. Acta* **2018**, *261*, 296–306. [CrossRef]

16. Li, Y.; Sniekers, J.; Malaquias, J.; Li, X.; Schaltin, S.; Stappers, L.; Binnemans, K.; Fransaer, J.; Vankelecom, I.F.J. A non-aqueous all-copper redox flow battery with highly soluble active species. *Electrochim. Acta* **2017**, *236*, 116–121. [CrossRef]

17. Hamelet, S.; Tzedakis, T.; Leriche, J.B.; Sailler, S.; Larcher, D.; Taberna, P.L.; Simon, P.; Tarascon, J.M. Non-Aqueous Li-Based Redox Flow Batteries. *J. Electrochem. Soc.* **2012**, *159*, A1360–A1367. [CrossRef]

18. Hwang, B.; Park, M.S.; Kim, K. Ferrocene and cobaltocene derivatives for non-aqueous redox flow batteries. *ChemSusChem* **2015**, *8*, 310–314. [CrossRef]

19. Hu, B.; Hu, M.; Luo, J.; Liu, T.L. A Sr, Low Permeable TEMPO Catholyte for Aqueous Total Organic Redox Flow Batteries. *Adv. Energy Mater.* **2021**, *12*, 2102577. [CrossRef]

20. Brushett, F.R.; Vaughey, J.T.; Jansen, A.N. An All-Organic Non-aqueous Lithium-Ion Redox Flow Battery. *Adv. Energy Mater.* **2012**, *2*, 1390–1396. [CrossRef]

21. Yuan, J.; Pan, Z.-Z.; Jin, Y.; Qiu, Q.; Zhang, C.; Zhao, Y.; Li, Y. Membranes in non-aqueous redox flow battery: A review. *J. Power Sources* **2021**, *500*, 229983. [CrossRef]

22. Zhen, Y.; Zhang, C.; Yuan, J.; Zhao, Y.; Li, Y. A high-performance all-iron non-aqueous redox flow battery. *J. Power Sources* **2020**, *445*, 227331. [CrossRef]

23. Ding, Y.; Zhao, Y.; Li, Y.; Goodenough, J.B.; Yu, G. A high-performance all-metallocene-based, non-aqueous redox flow battery. *Energy Environ. Sci.* **2017**, *10*, 491–497. [CrossRef]

24. Winsberg, J.; Hagemann, T.; Janoschka, T.; Hager, M.D.; Schubert, U.S. Redox-Flow Batteries: From Metals to Organic Redox-Active Materials. *Angew. Chem. Int. Ed. Engl.* **2017**, *56*, 686–711. [CrossRef] [PubMed]

25. Li, Y.; Geysens, P.; Zhang, X.; Sniekers, J.; Fransaer, J.; Binnemans, K.; Vankelecom, I.F.J. Cerium-containing complexes for low-cost, non-aqueous redox flow batteries (RFBs). *J. Power Sources* **2020**, *450*, 227634. [CrossRef]

26. Shoaib, M.; Vallayil, P.; Jaiswal, N.; Iyapazham Vaigunda Suba, P.; Sankararaman, S.; Ramanujam, K.; Thangadurai, V. Advances in Redox Flow Batteries—A Comprehensive Review on Inorganic and Organic Electrolytes and Engineering Perspectives. *Adv. Energy Mater.* **2024**, *14*, 2400721. [CrossRef]

27. Liu, Y.; Niu, Y.; Ouyang, X.; Guo, C.; Han, P.; Zhou, R.; Heydari, A.; Zhou, Y.; Ikkala, O.; Tigranovich, G.A.; et al. Progress of organic, inorganic redox flow battery and mechanism of electrode reaction. *Nano Res. Energy* **2023**, *2*, e9120081. [CrossRef]

28. Archana, K.S.; Suresh, S.; Ragupathy, P.; Ulaganathan, M. Investigations on new Fe–Mn redox couple based aqueous redox flow battery. *Electrochim. Acta* **2020**, *345*, 136245. [CrossRef]

29. Chakrabarti, B.K.; Ouyang, M.; Alkhateab, B.; Rubio-Garcia, J.; Dönmez, K.B.; Çobandede, Z.; Afshar Ghotli, R.; Soytaş, S.H.; Bayazıt, M.K.; Hajimolana, Y.S.; et al. Enhancement in the performance of a vanadium-manganese redox flow battery using electrospun carbon metal-based electrode catalysts. *Mater. Res. Bull.* **2025**, *182*, 113140. [CrossRef]

30. Ding, M.; Fu, H.; Lou, X.; He, M.; Chen, B.; Han, Z.; Chu, S.; Lu, B.; Zhou, G.; Jia, C. A Stable and Energy-Dense Polysulfide/Permanganate Flow Battery. *ACS Nano* **2023**, *17*, 16252–16263. [CrossRef] [PubMed]

31. Kim, B.; Kim, Y.S.; Dulyawat, D.; Chung, C.-H. Development of a Zn-Mn aqueous redox-flow battery operable at 2.4 V of discharging potential in a hybrid cell with an Ag-decorated carbon-felt electrode. *J. Energy Storage* **2023**, *72*, 108337. [CrossRef]

32. Lei, J.F.; Yao, Y.X.; Huang, Y.Q.; Lu, Y.C. A Highly Reversible Low-Cost Aqueous Sulfur-Manganese Redox Flow Battery. *ACS Energy Lett.* **2022**, *8*, 429–435. [CrossRef]

33. Liu, Y.; Nan, M.; Zhao, Z.; Shen, B.; Qiao, L.; Zhang, H.; Ma, X. Manganese-based flow battery based on the MnCl2 electrolyte for energy storage. *Chem. Eng. J.* **2023**, *465*, 142602. [CrossRef]

34. Nan, M.; Qiao, L.; Liu, Y.; Zhang, H.; Ma, X. Improved titanium-manganese flow battery with high capacity and high stability. *J. Power Sources* **2022**, *522*, 230995. [CrossRef]

35. Reynard, D.; Maye, S.; Peljo, P.; Chanda, V.; Girault, H.H.; Gentil, S. Vanadium-Manganese Redox Flow Battery: Study of Mn(III) Disproportionation in the Presence of Other Metallic Ions. *Chemistry* **2020**, *26*, 7250–7257. [CrossRef]

36. Sleightholme, A.E.S.; Shinkle, A.A.; Liu, Q.; Li, Y.; Monroe, C.W.; Thompson, L.T. Non-aqueous manganese acetylacetonate electrolyte for redox flow batteries. *J. Power Sources* **2011**, *196*, 5742–5745. [CrossRef]

37. Xiang, W.; Yang, M.; Ding, M.; Chen, X.; Liu, J.; Zhou, G.; Jia, C.; Waterhouse, G.I.N. Alkaline Zn-Mn aqueous flow batteries with ultrahigh voltage and energy density. *Energy Storage Mater.* **2023**, *61*, 102894. [CrossRef]

38. Cao, J.; Yu, K.; Zhang, J.; Lu, B.; Yu, J.; Huang, S.; Zhang, F. Vanadium-Mediated High Areal Capacity Zinc–Manganese Redox Flow Battery. *ACS Sustain. Chem. Eng.* **2024**, *12*, 6320–6329. [CrossRef]

39. Chaurasia, S.; Aravamuthan, S.R.; Sullivan, C.; Ross, M.B.; Agar, E. Investigating Manganese–Vanadium Redox Flow Batteries for Energy Storage and Subsequent Hydrogen Generation. *ACS Appl. Energy Mater.* **2024**, *7*, 11429–11441. [CrossRef]

40. Dong, Y.-R.; Kaku, H.; Hanafusa, K.; Moriuchi, K.; Shigematsu, T. A Novel Titanium/Manganese Redox Flow Battery. *ECS Trans.* **2015**, *69*, 59. [CrossRef]

41. Qiao, L.; Xie, C.; Nan, M.; Zhang, H.; Ma, X.; Li, X. Highly stable titanium–manganese single flow batteries for stationary energy storage. *J. Mater. Chem. A* **2021**, *9*, 12606–12611. [CrossRef]

42. Reynard, D.; Girault, H. Combined hydrogen production and electricity storage using a vanadium-manganese redox dual-flow battery. *Cell Rep. Phys. Sci.* **2021**, *2*, 100556. [CrossRef]

43. Li, Z.; Weng, G.; Zou, Q.; Cong, G.; Lu, Y.-C. A high-energy and low-cost polysulfide/iodide redox flow battery. *Nano Energy* **2016**, *30*, 283–292. [CrossRef]

44. Chen, H.; Zhang, X.; Zhang, S.; Wu, S.; Chen, F.; Xu, J. A comparative study of iron-vanadium and all-vanadium flow battery for large scale energy storage. *Chem. Eng. J.* **2022**, *429*, 132403. [CrossRef]

45. Chen, M.-L.; Huang, S.-L.; Hsieh, C.-L.; Lee, J.-Y.; Tsai, T.-J. Development of a Novel Iodine-Vitamin C/Vanadium Redox Flow Battery. *Electrochim. Acta* **2014**, *141*, 241–247. [CrossRef]

46. Chen, T.-S.; Huang, S.-L.; Chen, M.-L.; Tsai, T.-J.; Lin, Y.-S. Improving Electrochemical Activity in a Semi-V-I Redox Flow Battery by Using a C–TiO2–Pd Composite Electrode. *J. Nanomater.* **2019**, *2019*, 7460856. [CrossRef]

47. Huo, X.; Shi, X.; Bai, Y.; Zeng, Y.; An, L. A vanadium-chromium redox flow battery toward sustainable energy storage. *Cell Rep. Phys. Sci.* **2024**, *5*, 101782. [CrossRef]

48. Leung, P.K.; Mohamed, M.R.; Shah, A.A.; Xu, Q.; Conde-Duran, M.B. A mixed acid based vanadium–cerium redox flow battery with a zero-gap serpentine architecture. *J. Power Sources* **2015**, *274*, 651–658. [CrossRef]

49. Li, B.; Li, L.; Wang, W.; Nie, Z.; Chen, B.; Wei, X.; Luo, Q.; Yang, Z.; Sprenkle, V. Fe/V redox flow battery electrolyte investigation and optimization. *J. Power Sources* **2013**, *229*, 1–5. [CrossRef]

50. Muthuraman, G.; Silambarasan, P.; Bae, K.; Moon, I.S. Combination of Acid-Base Electrolyte at Each Half-Cell with a Single Zeolite Membrane for Crossover Free and Possible Increased Energy Density in an All Aqueous Redox Flow Battery. *J. Electrochem. Soc.* **2021**, *168*, 020531. [CrossRef]

51. Poon, G.; Parasuraman, A.; Lim, T.M.; Skyllas-Kazacos, M. Evaluation of N-ethyl-N-methyl-morpholinium bromide and N-ethyl-N-methyl-pyrrolidinium bromide as bromine complexing agents in vanadium bromide redox flow batteries. *Electrochim. Acta* **2013**, *107*, 388–396. [CrossRef]

52. Skyllas-Kazacos, M. Novel vanadium chloride/polyhalide redox flow battery. *J. Power Sources* **2003**, *124*, 299–302. [CrossRef]

53. Ulaganathan, M.; Suresh, S.; Mariyappan, K.; Periasamy, P.; Pitchai, R. New Zinc–Vanadium (Zn–V) Hybrid Redox Flow Battery: High-Voltage and Energy-Efficient Advanced Energy Storage System. *ACS Sustain. Chem. Eng.* **2019**, *7*, 6053–6060. [CrossRef]

54. Vafiadis, H.; Skyllas-Kazacos, M. Evaluation of membranes for the novel vanadium bromine redox flow cell. *J. Membr. Sci.* **2006**, *279*, 394–402. [CrossRef]

55. Wang, W.; Nie, Z.; Chen, B.; Chen, F.; Luo, Q.; Wei, X.; Xia, G.G.; Skyllas-Kazacos, M.; Li, L.; Yang, Z. A New Fe/V Redox Flow Battery Using a Sulfuric/Chloric Mixed-Acid Supporting Electrolyte. *Adv. Energy Mater.* **2012**, *2*, 487–493. [CrossRef]

56. Zeng, Y.K.; Zhao, T.S.; An, L.; Zhou, X.L.; Wei, L. A comparative study of all-vanadium and iron-chromium redox flow batteries for large-scale energy storage. *J. Power Sources* **2015**, *300*, 438–443. [CrossRef]

57. Chang, S.; Ye, J.; Zhou, W.; Wu, C.; Ding, M.; Long, Y.; Cheng, Y.; Jia, C. A low-cost SPEEK-K type membrane for neutral aqueous zinc-iron redox flow battery. *Surf. Coat. Technol.* **2019**, *358*, 190–194. [CrossRef]

58. Gong, K.; Ma, X.; Conforti, K.M.; Kuttler, K.J.; Grunewald, J.B.; Yeager, K.L.; Bazant, M.Z.; Gu, S.; Yan, Y. A zinc–iron redox-flow battery under $100 per kW h of system capital cost. *Energy Environ. Sci.* **2015**, *8*, 2941–2945. [CrossRef]

59. Kabtamu, D.M.; Lin, G.Y.; Chang, Y.C.; Chen, H.Y.; Huang, H.C.; Hsu, N.Y.; Chou, Y.S.; Wei, H.J.; Wang, C.H. The effect of adding Bi(3+) on the performance of a newly developed iron-copper redox flow battery. *RSC Adv* **2018**, *8*, 8537–8543. [CrossRef]

60. Manohar, A.K.; Kim, K.M.; Plichta, E.; Hendrickson, M.; Rawlings, S.; Narayanan, S.R. A High Efficiency Iron-Chloride Redox Flow Battery for Large-Scale Energy Storage. *J. Electrochem. Soc.* **2015**, *163*, A5118–A5125. [CrossRef]

61. Yu, S.; Yue, X.; Holoubek, J.; Xing, X.; Pan, E.; Pascal, T.; Liu, P. A low-cost sulfate-based all iron redox flow battery. *J. Power Sources* **2021**, *513*, 230457. [CrossRef]

62. Zeng, Y.K.; Zhao, T.S.; Zhou, X.L.; Wei, L.; Jiang, H.R. A low-cost iron-cadmium redox flow battery for large-scale energy storage. *J. Power Sources* **2016**, *330*, 55–60. [CrossRef]

63. Zeng, Y.K.; Zhao, T.S.; Zhou, X.L.; Wei, L.; Ren, Y.X. A novel iron-lead redox flow battery for large-scale energy storage. *J. Power Sources* **2017**, *346*, 97–102. [CrossRef]

64. Zhang, S.; Gao, S.; Zhang, Y.; Song, Y.; Gentle, I.R.; Wang, L.; Luo, B. All-soluble all-iron aqueous redox flow batteries: Towards sustainable energy storage. *Energy Storage Mater.* **2025**, *75*, 104004. [CrossRef]

65. Zou, H.; Xu, Z.; Xiong, L.; Wang, J.; Fu, H.; Cao, J.; Ding, M.; Wang, X.; Jia, C. An alkaline S/Fe redox flow battery endowed with high volumetric-capacity and long cycle-life. *J. Power Sources* **2024**, *591*, 233856. [CrossRef]

66. Amini, K.; Pritzker, M.D. Improvement of zinc-cerium redox flow batteries using mixed methanesulfonate-chloride negative electrolyte. *Appl. Energy* **2019**, *255*, 113894. [CrossRef]

67. Amini, K.; Pritzker, M.D. Life-cycle analysis of zinc-cerium redox flow batteries. *Electrochim. Acta* **2020**, *356*, 136785. [CrossRef]

68. Kocyigit, N.; Gencten, M.; Sahin, M.; Sahin, Y. A novel electrolytes for redox flow batteries: Cerium and chromium couples in aqueous system. *Int. J. Energy Res.* **2021**, *45*, 16176–16188. [CrossRef]

69. Leung, P.K.; Ponce de León, C.; Walsh, F.C. An undivided zinc–cerium redox flow battery operating at room temperature (295 K). *Electrochem. Commun.* **2011**, *13*, 770–773. [CrossRef]

70. Na, Z.; Xu, S.; Yin, D.; Wang, L. A cerium–lead redox flow battery system employing supporting electrolyte of methanesulfonic acid. *J. Power Sources* **2015**, *295*, 28–32. [CrossRef]

71. Nikiforidis, G.; Berlouis, L.; Hall, D.; Hodgson, D. Impact of electrolyte composition on the performance of the zinc–cerium redox flow battery system. *J. Power Sources* **2013**, *243*, 691–698. [CrossRef]

72. Nikiforidis, G.; Berlouis, L.; Hall, D.; Hodgson, D. An electrochemical study on the positive electrode side of the zinc–cerium hybrid redox flow battery. *Electrochim. Acta* **2014**, *115*, 621–629. [CrossRef]

73. Nikiforidis, G.; Daoud, W.A. Effect of Mixed Acid Media on the Positive Side of the Hybrid Zinc-Cerium Redox Flow Battery. *Electrochim. Acta* **2014**, *141*, 255–262. [CrossRef]

74. Silambarasan, P.; Ramu, A.G.; Govarthanan, M.; Kim, W.; Moon, I.S. Cerium-polysulfide redox flow battery with possible high energy density enabled by MFI-Zeolite membrane working with acid-base electrolytes. *Chemosphere* **2022**, *291 Pt 1*, 132680. [CrossRef]

75. Wu, Y.; Zhou, L.; Xie, Y.; Lai, Y.; Fu, S.; Kang, X.; Shi, W.; Li, J.; Zhang, X.; Hu, K.; et al. A green europium-cerium redox flow battery with ultrahigh voltage and high performance. *Chem. Eng. J.* **2024**, *500*, 157189. [CrossRef]

76. Zeng, D.; Mao, T.; Zhang, Z.; Dai, J.; Ouyang, J.; Xie, Z. A high-performance aqueous Eu/Ce redox flow battery for large-scale energy storage application. *Int. J. Heat Mass Transf.* **2024**, *233*, 125978. [CrossRef]

77. Asadipour, E.; Sahadevan, S.A.; Ramani, V. Polymer-blended and reinforced anion-exchange membranes for methanesulfonic acid-based titanium–cerium redox flow batteries. *J. Membr. Sci.* **2025**, *718*, 123696. [CrossRef]

78. Kellamis, C.J.; Wainright, J.S. A zinc–iodine hybrid flow battery with enhanced energy storage capacity. *J. Power Sources* **2024**, *589*, 233753. [CrossRef]

79. Li, B.; Nie, Z.; Vijayakumar, M.; Li, G.; Liu, J.; Sprenkle, V.; Wang, W. Ambipolar zinc-polyiodide electrolyte for a high-energy density aqueous redox flow battery. *Nat. Commun.* **2015**, *6*, 6303. [CrossRef]

80. Wu, M.C.; Zhao, T.S.; Wei, L.; Jiang, H.R.; Zhang, R.H. Improved electrolyte for zinc-bromine flow batteries. *J. Power Sources* **2018**, *384*, 232–239. [CrossRef]

81. Xie, C.; Zhang, H.; Xu, W.; Wang, W.; Li, X. A Long Cycle Life, Self-Healing Zinc-Iodine Flow Battery with High Power Density. *Angew. Chem. Int. Ed. Engl.* **2018**, *57*, 11171–11176. [CrossRef] [PubMed]

82. Xu, Z.; Li, J.; Wu, M. A high-rate and long-life zinc-bromine flow battery. *J. Power Sources* **2024**, *613*, 234869. [CrossRef]

83. Zeng, Y.; Yang, Z.; Lu, F.; Xie, Y. A novel tin-bromine redox flow battery for large-scale energy storage. *Appl. Energy* **2019**, *255*, 113756. [CrossRef]

84. Zhang, L.; Zhang, H.; Lai, Q.; Li, X.; Cheng, Y. Development of carbon coated membrane for zinc/bromine flow battery with high power density. *J. Power Sources* **2013**, *227*, 41–47. [CrossRef]